A two-band model for the phase separation induced by the chemical mismatch pressure in different cuprate superconductors

Supercond. Sci. Technol. **22** (2009) 014007 (7pp) doi:10.1088/0953-2048/22/1/014007

A two-band model for the phase separation induced by the chemical mismatch pressure in different cuprate superconductors

K I Kugel[1,2], A L Rakhmanov[1,2], A O Sboychakov[1], F V Kusmartsev[2], Nicola Poccia[3] and Antonio Bianconi[3]

[1] Institute for Theoretical and Applied Electrodynamics, Russian Academy of Sciences, Izhorskaya Street 13, Moscow, 125412, Russia
[2] Department of Physics, Loughborough University, Loughborough LE11 3TU, UK
[3] Department of Physics, University of Rome 'La Sapienza', Piazzale Aldo Moro 2, 00185 Rome, Italy

E-mail: kugel@orc.ru

Received 13 June 2008, in final form 21 August 2008
Published 16 December 2008
Online at stacks.iop.org/SUST/22/014007

Abstract
A two-band model is used to study the phase separation in systems with different kinds of strongly correlated charge carrier, with a special emphasis on cuprate superconductors near optimum doping. We show that such a system can decompose into two metallic-like phases with more and less localized carriers. This phase separation is controlled by the energy splitting between the two bands. In cuprate superconductors, this energy splitting can be related to the internal chemical pressure on the CuO_2 layer due to interlayer mismatch. The interplay between the surface energy of nanoscale inhomogeneities and the long-range Coulomb interaction determines the geometry of the phase-separated state (droplet- or stripe-like, depending on doping). The model is able to reproduce the regime of phase separation at doping higher than $1/8$ in the experimental pressure–doping–T_c phase diagram of cuprates at large microstrain as it appears in superoxygenated La_2CuO_4.

(Some figures in this article are in colour only in the electronic version)

1. Introduction

Recent experiments with angle-resolved photoemission spectroscopy (ARPES) [1–5] and scanning tunneling spectroscopy (STM) [6, 7] provide compelling experimental evidence for the dual nature of charge carriers and the nanoscale phase separation of the two components in two different spatial domains in cuprate high-T_c superconductors [8–10]. A clear case for the phase separation of the two types of charge carrier is overoxygenated La_2CuO_{4+y}, where the interstitial oxygen ions are mobile above 180 K and stimulate the phase separation of the two different kinds of dopant hole [11–19]. Currently, from the analysis of magnetic neutron scattering experiments, there is an agreement for the frustrated mesoscopic phase separation at doping larger than $1/8$ in Sr-doped La214, Y123, and Bi2212 between a first more delocalized component that does not show spin fluctuations and a second more localized electronic component, showing stripe-like spin fluctuations [20, 21]. Several reviews and books have been published on the two-component scenario and phase separation in cuprates [17–19, 22–25]. Here we focus not on the well studied phase separation in the underdoped regime, near the Mott phase, between a hole-poor antiferromagnetic phase and a metallic hole-rich phase but on the phase separation in the overdoped regime [11–21] between a hole-poor phase with doping close to $1/8$ and a hole-rich phase with doping close to $1/4$. A similar scenario is now well accepted for understanding the physics of phase separation in manganites [26–28]. It was shown that even in the absence of any specific order parameter, the presence of two strongly correlated electronic bands leads to the possibility of a phase-separated state [29].

Here we consider a theoretical model of the mesoscopic phase separation in a two-band scenario of two strongly correlated electronic fluids. Below, we show that this simple model grabs the key physics of the anomalous normal phase in cuprates exhibiting phase separation as a function of charge density and the energy splitting between the two bands. This allows the understanding of the different superconducting phases in different cuprate families, i.e., the new 3D phase diagram where the critical temperature depends on the doping and pressure [30].

In fact, there are two types of phase separation discussed in the physics community for cuprates. The first scenario considers a single band at low doping (less than 1/8) in the CuO_2 layers. This classical stripe scenario shows an atomic-scale stripe phase separation resulting from frustrated phase separation in the case of static randomly distributed chemical dopants in the intercalated layers (spacers) like LaSrCuO as a prototype. In this standard stripe model, a hole-rich atomic stripe (with 0.5 holes per Cu) forms an antiphase boundary between the undoped antiferromagnetic striped regions made of three Cu rows. In this regime, by increasing the doping, the period of the striped superlattice decreases up to the lowest period of four atomic rows corresponding to 1/8 doping. The second scenario of phase separation is a so-called Swiss-cheese model [14] for doping larger than 1/8. In this macroscopic phase separation, the hole-poor magnetic stripe-ordered region (with doping close to 1/8) (pseudo-gap matter) is separated from the hole-rich metallic region (with larger doping, about 1/4). In our paper, we describe a two-band theoretical model that provides evidence for the second macroscopic phase separation scenario. In the present phase separation scenario, bubbles of a hole-poor phase (with doping close to 1/8) coexist with bubbles of a hole-rich phase (with doping larger than 1/4).

Earlier, the evolution of phase separation was studied as a function of doping within a two-band scenario [29]. However, a large amount of data clearly indicates that the phase separation regime is not only a function of doping but also of the anisotropic chemical pressure acting on the CuO_2 layers, due to interlayer mismatch [31–34]. The chemical pressure is a well established physical variable that controls the physical properties of perovskites and it is usually measured by the average ionic radius of the cations in the intercalated layers or the tolerance factor t; in fact, the internal chemical pressure in perovskites can be defined as $\eta = 1 - t$. In all perovskites, and particularly in manganites, it is well established that the phase diagram of the electronic phases depends on the two variables, charge density and chemical pressure [35]. Since the early years of high-T_c superconductivity research, the mismatch chemical pressure has been considered as a key variable controlling the electronic properties of cuprates only in one family, La214 [34]; however, it was not possible to extend this idea to other families for the presence of a plurality of intercalated layers with cations having largely different coordination numbers. Therefore, it was not possible to compare the average ionic size $\langle r_A \rangle$ in the intercalated layers and to get the tolerance factor t for all cuprate families. This problem was solved by obtaining the internal chemical pressure from the measure of the compressive microstrain $\varepsilon = (R_0 - r)/r$ in the CuO_2 plane (that has the same absolute value as the tensile microstrain in the intercalated layers) where r is the average Cu–O distance and $R_0 = 0.197$ nm is the unrelaxed Cu–O distance [31–33]. Therefore, the chemical pressure is proportional to the microstrain, $\eta = 2\varepsilon$.

In section 2, we formulate a model of a two-component system made of two different strongly correlated electron bands. In section 3, we analyze the region of the phase separation state in the band-shift–doping plane. Here we also discuss the possible geometry of the phase-separated state, taking into account the surface and long-range Coulomb energies of nanoscale inhomogeneities. In section 4, arguing that the energy splitting between the two bands is controlled by the chemical pressure, we analyze the relation between the theoretical phase diagram and the experimental 3D phase diagram of cuprates.

2. The model

We describe the system with the two types of strongly correlated charge carrier characteristic of cuprates in terms of the two-band Hubbard model. The Hamiltonian of such a system can be written as [29]

$$H = -\sum_{\langle \mathbf{nm}\rangle \alpha,\sigma} t_\alpha a^\dagger_{\mathbf{n}\alpha\sigma} a_{\mathbf{m}\alpha\sigma} - \Delta E \sum_{\mathbf{n}\sigma} n_{\mathbf{n}b\sigma} - \mu \sum_{\mathbf{n}\alpha,\sigma} n_{\mathbf{n}\alpha\sigma} + \frac{1}{2}\sum_{\mathbf{n}\alpha,\sigma} U^\alpha n_{\mathbf{n}\alpha\sigma} n_{\mathbf{n}\alpha\bar{\sigma}} + \frac{U'}{2}\sum_{\mathbf{n}\alpha,\sigma\sigma'} n_{\mathbf{n}\alpha\sigma} n_{\mathbf{n}\bar{\alpha}\sigma'}. \quad (1)$$

Here, $a^\dagger_{\mathbf{n}\alpha\sigma}$ and $a_{\mathbf{n}\alpha\sigma}$ are the creation and annihilation operators for electrons corresponding to bands $\alpha = \{a, b\}$ at site $\mathbf{n}$ with spin projection σ, and $n_{\mathbf{n}\alpha\sigma} = a^\dagger_{\mathbf{n}\alpha\sigma} a_{\mathbf{n}\alpha\sigma}$. The symbol $\langle \cdots \rangle$ denotes summation over the nearest-neighbor sites. The first term on the right-hand side of equation (1) corresponds to the kinetic energy of the conduction electrons in bands a and b with the hopping integrals $t_a > t_b$. In our model, we ignore the interband hopping. The second term describes the shift ΔE of the center of band b with respect to the center of band a ($\Delta E > 0$ if the center of band b is below the center of band a). The last two terms describe the on-site Coulomb repulsion of two electrons either in the same state (with Coulomb energy U^α) or in different states (U'). The bar above α or σ denotes *not* α or *not* σ, respectively. The assumption of strong electron correlations means that the Coulomb interaction is large; that is, $U^\alpha,\ U' \gg t_\alpha,\ \Delta E$. The total number n of electrons per site is the sum of electrons in the a and b states, $n = n_a + n_b$, and μ is the chemical potential. Below, we consider the case $n \leqslant 1$ relevant to cuprates.

The model equation (1) predicts a tendency to phase separation in a certain range of parameters: in particular, in the case when the hopping integrals for the a and b bands differ significantly ($t_a > t_b$) [29]. This tendency results from the effect of strong correlations giving rise to the dependence of the width of one band on the filling of another band. In the absence of the electron correlations ($n \ll 1$), the half-width $w_a = zt_a$ of the a band is larger than $w_b = zt_b$ (z is the number of the nearest neighbors of the copper ion). Due to the electron correlations, the relative widths of the a and b bands can vary significantly [29]. Using the Hubbard I approximation in the

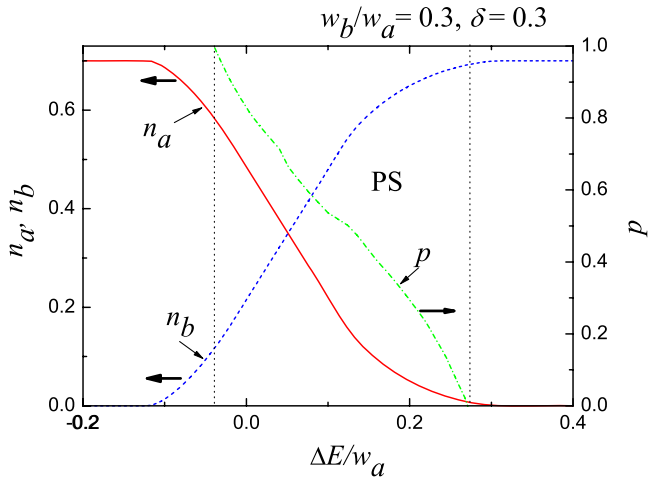

Figure 1. Evolution of the occupation numbers n_a and n_b of the bands a and b at fixed doping $\delta = 0.3$ in the absence of phase separation. The region of phase separation lies between the two vertical dotted lines. There we have two phases: P_a, including mostly a charge carriers, and P_b, with dominant b carriers. The content of different types of carrier in P_a and P_b is given by the intersections of the n_a and n_b curves with the left and right dashed vertical curves, respectively. The change in concentration p of phase P_a in the phase separation region is shown by the (green) dot–dashed line.

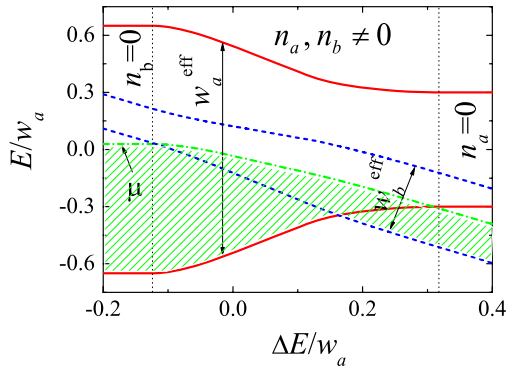

Figure 2. Effective widths $w_{a,b}^{\rm eff}$ of the a and b bands versus band shift ΔE at fixed doping $\delta = 0.3$. The (green) dot–dashed curve illustrates the behavior of the chemical potential μ; the (green) hatched area under this curve corresponds to the states occupied by charge carriers.

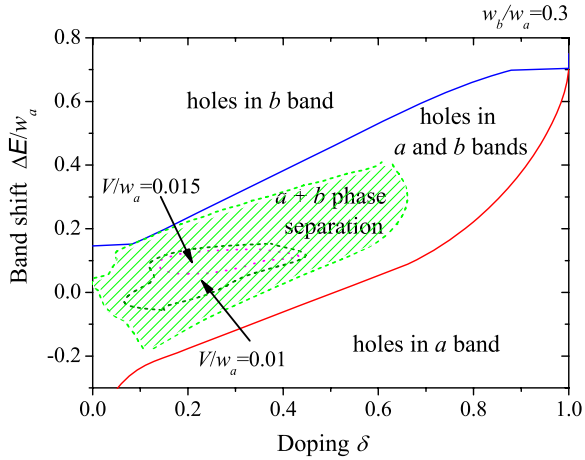

Figure 3. The phase diagram of model (1) in the doping–band-shift plane at the ratio of band widths $w_b/w_a = 0.3$. Below the lower (red) solid line, there are charge carriers only of a type, whereas above the upper (blue) curve there are only b carriers. Between these lines, there appears the region of phase separation (marked by (green) hatching). The charge disproportionalization in the phase-separated state can substantially reduce this region: the arrows indicate the phase separation regions at $V/w_a = 0.01$ and 0.015, where V is the characteristic energy of intersite Coulomb interaction.

limit $U^\alpha, U' \to \infty$, we can describe the evolution of the band structure with the change of n and ΔE following the method presented in [29]. Analysis of the system energy reveals the possibility of the inhomogeneous state consisting of domains having different charge carrier densities n_1 and n_2. The ratio of the numbers of a and b carriers is different in different phases. In the first phase, P_a, almost all charge carriers are in the band a, while in the second phase, P_b, the situation is opposite.

The undoped state of the cuprates corresponds to one electron per site ($n = 1$) in the model used in [29]. The number of itinerant holes δ is related to n as $\delta = 1 - n$. In general, the relationship between n and δ could be more complicated [36]; however, for the present considerations such corrections are not of principal importance.

3. Phase-separated state

3.1. Regions of phase separation

The analysis of the model (1) was performed in [29] in the Hubbard I approximation. Based on this analysis, it can be shown that due to the strong electron correlations the filling of band a depends on the filling of band b and vice versa. The evolution of the occupation numbers n_a and n_b of the two bands with ΔE at a fixed doping is illustrated in figure 1. Note also that the effective widths of the a and b bands vary with the band shift due to the electron correlation effects. This is illustrated in figure 2.

The phase diagram in the $(\delta, \Delta E)$ plane is drawn in figure 3. In this figure, below the lower (red) solid line, we have the charge carriers only of a type, whereas above the upper (blue) curve, there are only b carriers. If we ignore the possibility of phase separation, the relative number of a and b charge carriers varies gradually between these two lines. Taking into account possible phase-separated states results in a significant modification of the phase diagram in the range of intermediate doping. In the hatched (green) region in figure 3 the homogeneous state becomes unfavorable and the system separates into two phases (P_a and P_b) with different numbers of charge carriers per site, $n_1 \approx n_a$ and $n_2 \approx n_b$. The electrostatic contribution to the energy related to an inhomogeneous charge distribution reduces the doping range, in which phase separation is favorable [29]. In figure 3, we illustrate that a relatively small energy loss due to the charge disproportionalization leads to a substantial decrease in the area of the phase separation region: compare the areas indicated by arrows corresponding to $V/w_a = 0.01$ and 0.015 (V is the characteristic energy of intersite Coulomb

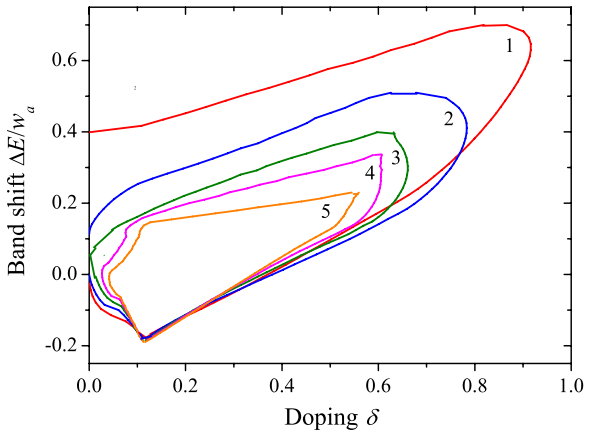

Figure 4. The phase separation regions given by model (1) at $V = 0$ and different values of the bandwidth ratio: $w_b/w_a = 0.1$ (curve 1), 0.2 (2), 0.3 (3), 0.35 (4), and 0.4 (5). At $w_b/w_a > 0.4$, the phase separation is unfavorable in energy.

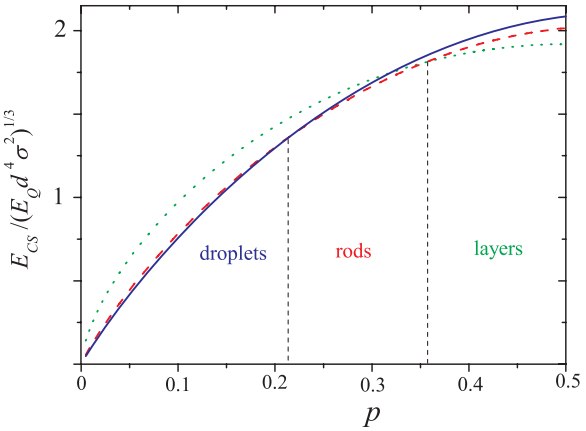

Figure 5. Normalized energy of an inhomogeneity as a function of the phase content p at $p < 0.5$. The picture for $p > 0.5$ is a mirror reflection of this figure with respect to the vertical line $p = 0.5$. Solid (blue), dashed (red), and dotted (green) lines correspond to droplets, rods, and planes, respectively.

interaction [29]) and the whole hatched area corresponding to $V = 0$. Note that, at low hole doping (n close to one), the antiferromagnetic (AF) correlations are dominant, which requires a special analysis. The phase-separated state arises in the two-band model (1) at small values of the bandwidth ratio w_b/w_a. The evolution of the phase separation region in the $(\delta, \Delta E)$ plane with the change of w_b/w_a is shown in figure 4. This region shrinks rapidly with the increase of w_b/w_a and disappears if $w_b/w_a > 0.4$, where the phase separation becomes unfavorable in energy.

3.2. Geometry of the phase-separated state

Phase separation occurs in the range of parameters where the energy of the homogeneous state as a function of doping has a negative curvature corresponding to the negative compressibility [28, 29]. Determining the region of phase separation in figure 3 at non-zero contribution of the long-range Coulomb interaction V to the energy of the phase-separated state, we assumed the simplest droplet-like geometry of the inhomogeneities. However, it has been widely discussed in the literature that long-range Coulomb interaction in systems with negative compressibility can give rise to more complicated geometry of phase separation (stripes, layers, rods, etc); see [37, 38] and references therein. Below we demonstrate that the energy difference between different geometries is relatively small (see figure 5).

The geometry of the phase-separated state is determined by the interplay of the surface energy of inhomogeneities and the long-range Coulomb interaction. Let us calculate the Coulomb contribution to the total energy for different shapes of inhomogeneities: spherical ($D = 3$), cylindrical ($D = 2$), and layered ($D = 1$). The geometry of the system will be considered in the Wigner–Seitz approximation; that is, the system is divided into cells, where an internal region (core) of the phase P_a is surrounded by a shell of phase P_b, if the concentration p of phase P_a is lower than 0.5, and vice versa if $p > 0.5$. The relative volumes of the core and shell are determined by p found by the electroneutrality condition

$$n_1 p + n_2(1 - p) = 1 - \delta. \tag{2}$$

We assume that the characteristic sizes of inhomogeneities are larger than the lattice constant d and use the macroscopic approach to calculate the electrostatic energy. We do not consider the interaction between neutral cells and take into account the screening of the Coulomb interaction by introducing the macroscopic dielectric constant.

We denote the size of the core as R_s, which is the radius of the internal sphere or cylinder in 3D or 2D cases, respectively, and the half-width of the internal layer in the 1D case. Following the approach of [39, 40], we can write the Coulomb energy per unit cell in the form

$$E_C^D = E_Q \left(\frac{R_s}{d}\right)^2 u_D(p), \tag{3}$$

where $E_Q = e^2(n_1 - n_2)^2/\epsilon d$, ϵ is the average permittivity, and $u_D(p)$ is a dimensionless function depending on the geometry of the system. At $p < 0.5$, we obtain

$$u_3(p) = \frac{4\pi p}{5}\left(2 - 3p^{1/3} + p\right), \qquad \text{spherical geometry}$$
$$D = 3 \text{ (droplets)}, \tag{4}$$
$$u_2(p) = \pi p\,(-\ln p + p - 1), \qquad \text{cylindrical geometry}$$
$$D = 2 \text{ (rods)}, \tag{5}$$
$$u_1(p) = \frac{4\pi}{3}(1 - p)^2, \qquad \text{layer geometry } D = 1. \tag{6}$$

In the case $p > 0.5$, we should use the replacements $n_1 \leftrightarrow n_2$ and $p \leftrightarrow 1 - p$.

For our system, the surface energy is determined by the size quantization [29]. At $R_s > d$, the surface tension $\sigma(n_1, n_2)$ does not depend on the shape of the inhomogeneities. Then, we can write the surface energy per unit cell as $E_\sigma^D = \sigma(n_1, n_2) S_D d^3/V_D$, where S_D is the surface area of the core

and V_D is the total volume of the Wigner–Seitz cell. Then, it is convenient to write

$$E_\sigma^{\mathrm{D}} = d^2\sigma(n_1, n_2)pD\frac{d}{R_{\mathrm{s}}}. \tag{7}$$

Minimizing the total energy $E_{\mathrm{CS}}^{\mathrm{D}} = E_\sigma^{\mathrm{D}} + E_C^{\mathrm{D}}$ with respect to R_{s}, we find

$$E_{\mathrm{CS}}^{\mathrm{D}}(p) = 3E_Q\left(\frac{d^2\sigma}{2E_Q}pD\sqrt{u_{\mathrm{D}}}\right)^{2/3}. \tag{8}$$

The behavior of energy $E_{\mathrm{CS}}^{\mathrm{D}}$ as function of p is illustrated in figure 5 at $p < 0.5$. We see that the droplet geometry is the most favorable in energy at small p ($p < p_1 = 0.215$). At intermediate values of p ($p_1 < p < p_2 = 0.355$), we have rods, which are transformed to layers at $p > p_2$. Note, however, that the different geometries are close in energy. The picture is symmetrical with respect to point $p = 0.5$.

The electroneutrality condition (2) determines the relationship between the phase content and doping $p = (1 - \delta - n_2)/(n_1 - n_2)$. In the main approximation, the values n_1 and n_2 are independent of doping. So, the phase content is a linear function of doping, and the inhomogeneities evolve with doping as follows. Phase separation arises if the doping exceeds some value $\delta = \delta^*(w_a/w_b, \Delta E) > 1 - n_2$. If $\delta^* < \delta_1 = 1 - n_1p_1 - n_2(1 - p_1)$, the phase separation appears in the form of nanoscale droplets of phase P_b in P_a. At $\delta_1 < \delta < \delta_2 = 1 - n_1p_2 - n_2(1 - p_2)$ the geometry changes to rod-like. At larger doping, $\delta > \delta_2$, we have the stripe-like layered configuration. If the value of δ^* becomes larger than δ_1 and/or δ_2, droplet-like or even rod-like structure can be missed.

Thus, due account of the long-range Coulomb interaction could reproduce different superstructures (stripes, in particular) observed in the cuprate superconductors near the optimum doping.

4. Results and discussion

Now let us discuss the relation of the above model to the experimental situation in the copper-based perovskites, where two types of charge carrier and an inhomogeneous (phase-separated) state are observed. The inhomogeneous state in cuprates corresponds to the coexistence of two phases. One of them is characterized by a superstructure (charge ordering, stripes, etc) and the other one has no superstructure. The state with charge (or spin) superstructure corresponds to a higher degree of localization and, therefore, to a smaller value of the hopping integral. Naturally, a charge carrier may hop either retaining short-range order and gaining in potential energy or hop in an arbitrary way with larger hopping integral thus gaining kinetic energy. The former corresponds to our b state and the latter to the a state. In our analysis, we did not consider any ordering, which arises in the next-order approximations. In particular, magnetic ordering requires taking into account terms of the order of $t_{a,b}^2/U$ and charge ordering implies allowing for the Coulomb interaction of carriers at different sites (nearest neighbor at least).

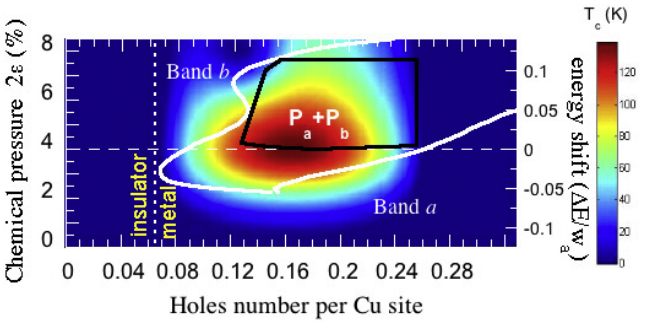

Figure 6. The values of the superconducting transition temperature T_{c} from 0 for dark blue to 135 K for dark red is shown in a color plot as a function of chemical pressure (2ε) and doping (holes number per Cu site). The white curve corresponds to the phase separation region given by the two-band Hubbard model (1) corresponding to $w_b/w_a = 0.3$ and $V/w_a = 0.01$ (see figure 3). Phases P_a and P_b include mostly carriers of a type and b type, respectively. The black solid line is the boundary of the phase-separated state deduced from neutron scattering and anomalous diffraction experiments for cuprates (La214, Bi2212, and Y123 systems).

The relative position of the two bands, ΔE, depends, in particular, on the chemical pressure proportional to the microstrain ε in the crystal lattice. To describe the experimental phase diagram of cuprates in the (δ, ε) plane [30–33], we should know the relationship between the band shift and the chemical pressure. It is natural to assume that these parameters are linearly related to each other, if $|\varepsilon| \ll 1$. Bearing this in mind, we compare the theoretical phase diagram in figure 3 with the experimental 3D phase diagram of cuprates [30, 31] in figure 6. The left-hand y scale is the mismatch chemical pressure η related to microstrain as $\eta = 2\varepsilon$ and the x axis is the doping (the number of holes per Cu site). The color plot represents the values of critical temperature in different superconducting cuprate families. The plot shows the fit of the experimental data of a large number of materials with the convolution of a parabolic curve with the maximum at $T_{\max}$ for T_{c} as a function of doping, and an asymmetric Lorentzian for $T_{\max}$ as a function of the mismatch chemical pressure with the maximum of 130 K at $2\varepsilon = 4\%$. The y axis in the right-hand side of the figure gives the energy distance ΔE between the center of band a and band b normalized to the width of band w_a of the more itinerant carriers. The phase diagram involving the superconducting critical temperature, chemical pressure, and doping reaches a T_{c} maximum at $2\varepsilon = 4\%$ and 0.16 holes per Cu sites. We can identify a low doping insulating phase, for any chemical pressure, at doping smaller than 0.06, where the vertical dashed line indicates the line of metal–insulator transition. The experimental investigations of the novel 3D phase diagram of cuprates indicate that the homogeneous metallic phase, with more delocalized states, occurs for both high doping and low chemical pressure, i.e., in the bottom-right corner of the figure. In this region, in the theoretical model we have charge carriers only in band a. In contrast, the homogeneous phase made of localized states where the striped phase appears occurs at the corner on the top-left side of the figure. In the theoretical model, we have in such a region charge carriers only in the band b.

The superconducting phase occurs in the intermediate region between these two limiting cases. The phase separation region predicted by our model (inside the area bounded by the solid white line) corresponds to the superconducting phase. This is in qualitative agreement with scanning tunneling microscopy (STM), EXAFS, and neutron pair distribution function (PDF) experiments showing that high-T_c superconductivity occurs in a regime of mesoscopic phase separation. The present results show that the maximum critical temperature occurs where the energy splitting between the more itinerant band a and the more localized band b is close to zero.

The theoretical phase diagram reproduces qualitatively the experimental results on phase separation in cuprates (La214, Bi2212, and Y123 systems) near optimum doping obtained by neutron scattering and anomalous diffraction techniques [31–33]. Phase separation arises in the intermediate doping range and disappears at low and high doping levels. The phase with 'more itinerant' electrons exists at small microstrains, the 'more localized' (and more ordered) phase arises at higher microstrains, and the phase-separated state is located in the intermediate range of ε.

We see that the experiment corresponds to relatively large values of the ratios w_b/w_a and V/w_a, where the region of phase separation is substantially reduced. As was shown in section 3.2, such a situation corresponds rather to the stripe-like geometry of the phase separation than to the droplets.

Our calculations predict phase separation in a broader doping range than in the experiments. This seems to be a consequence of simplifications used in the formulation and approximate analysis of the two-band Hubbard model (1). To improve the agreement with the experiment it is necessary to take into account specific features of the lattice and the electron structure of the cuprate superconductors. In particular, we disregard the interband electron transitions; that is, we neglect the terms $t_{ab}a^{\dagger}_{\mathbf{n}a\sigma}a_{\mathbf{m}b\sigma}$ in Hamiltonian (1) assuming that $t_{ab} = 0$. The doping range where phase separation can exist reduces with the increase of t_{ab} [41].

As follows from figure 6, the superconducting transition temperature T_c is the highest for the parameter range where the system is in the phase-separated state. This is an indication that the mechanism of phase separation is intimately related to the phenomenon of superconductivity. It is worth noting that in the case when the interband coupling t_{ab} is in the range $t_a < t_{ab} < t_b$, the electron density of states has a peak near the Fermi level in the parameter range corresponding to the phase-separated state, where T_c is maximum [41]. We cannot say whether this fact is accidental or not.

5. Conclusions

Up to now, most of the attention of both experimentalists and theorists has been addressed to phase separation in the underdoped regime between a first undoped antiferromagnetic phase and a second doped metallic phase of cuprates. Now, we have evidence for mesoscopic phase separation in the overdoped region of cuprate superconductors where a striped phase at doping $1/8$ coexists with a metallic phase with doping close to $1/4$. In our paper, we were dealing just with this situation.

We have presented an emerging theoretical scenario that relates the phase separation to the chemical pressure. This scenario grabs key physical aspects of the 3D phase diagram of cuprates. It was shown that the two-band model is appropriate for the normal phase of all cuprate superconducting families, where the energy splitting between the two bands is controlled by mismatch chemical pressure. In the regime where the two bands are close in energy, the system is unstable toward phase separation. The highest critical temperature of the superconducting transition in cuprates is attained within the phase-separated state.

Acknowledgments

The work was supported by the European project CoMePhS (contract NNP4-CT-2005-517039), International Science and Technology Center (grant G1335), and by the Russian Foundation for Basic Research, grants 08-02-00212 and 06-02-16691. AO also acknowledges support from the Russian Science Support Foundation.

References

[1] Lee W S, Vishik I M, Tanaka K, Lu D H, Sasagawa T, Nagaosa N, Deveraux T P, Hussain Z and Shen Z X 2007 *Nature* **450** 81
[2] Kondo T, Takeuchi T, Kaminski A, Tsuda S and Shin S 2007 *Phys. Rev. Lett.* **98** 267004
[3] Le Tacon M, Sacuto A, Georges A, Kotliar G, Gallais Y, Colson D and Forget A 2006 *Nat. Phys.* **2** 537
[4] Shen K M *et al* 2005 *Science* **307** 901
[5] Gweon G H, Sasagawa T, Zhou S Y, Graf J, Takagi H, Lee D-H and Lanzara A 2004 *Nature* **430** 187
[6] McElroy K, Lee J, Slezak J A, Lee D-H, Eisaki H, Uchida S and Davis J C 2005 *Science* **309** 1048
[7] Boyer M C, Wise W D, Chatterjee K, Yi M, Kondo T, Takeuchi T, Ikuta H and Hudson E W 2007 *Nat. Phys.* **3** 802
[8] Bianconi A, Saini N L, Lanzara A, Missori M, Rossetti T, Oyanagi H, Yamaguchi H, Oka K and Ito T 1996 *Phys. Rev. Lett.* **76** 3412
Bianconi A, Saini N L, Rossetti T, Lanzara A, Perali A, Missori M, Oyanagi H, Yamaguchi H, Nishihara Y and Ha D H 1996 *Phys. Rev.* B **54** 12018
[9] Müller K A, Zhao G-m, Conder K and Keller K 1998 *J. Phys.: Condens. Matter* **10** L291
[10] Bianconi A 1994 *Solid State Commun.* **91** 1
[11] Lee Y S, Birgeneau R J, Kastner M A, Endoh Y, Wakimoto S, Yamada K, Erwin R W, Lee S-H and Shirane G 1999 *Phys. Rev.* B **60** 3643
[12] Di Castro C, Colapietro M and Bianconi G 2000 *Int. J. Mod. Phys.* B **14** 3438
[13] Wen H H, Chen X H, Yang W L and Zhao Z H 2000 *Phys. Rev. Lett.* **85** 2805
[14] Uemura Y J 2001 *Solid State Commun.* **120** 347
[15] Savici A T *et al* 2002 *Phys. Rev.* B **66** 014524
[16] Mohottala H E, Wells B O, Budnick J I, Hines W A, Niedermayer C, Udby L, Bernhard C, Moodenaugh A R and Chou F C 2006 *Nat. Mater.* **5** 377
[17] Kusmartsev F V, Di Castro D, Bianconi G and Bianconi A 2000 *Phys. Lett.* A **275** 118
[18] Kivelson S A, Aeppli G and Emery V J 2000 *Proc. Natl Acad. Sci.* **98** 11903
[19] Kivelson S A 2006 *Nat. Mater.* **5** 343
[20] Birgeneau R J, Stock S, Tranquada J M and Yamada K 2006 *J. Phys. Soc. Japan* **75** 111003

[21] Tranquada J M 2007 *Handbook of High-Temperature Superconductivity* (New York: Springer) pp 257–98
[22] Müller K A 1999 *J. Supercond.* **12** 3
Müller K A 2000 *Physica* C **341–348** 11
[23] Müller K A and Bussmann-Holder A (ed) 2005 *Superconductivity in Complex Systems* (*Structure and Bonding* vol 114) (Berlin: Springer)
[24] Müller K A 2003 *Intrinsic MultiscaleStructure and Dynamics in Complex Electronic Oxides* ed A R Bishop, S R Shenoy and S Sridhar (Singapore: World Scientific)
[25] Müller K A 2000 in *Stripes and Related Phenomena* ed A Bianconi and N L Saini (New York: Kluwer)
[26] Dagotto E 2003 *Nanoscale Phase Separation and Colossal Magnetoresistance: The Physics of Manganites and Related Compounds* (Berlin: Springer)
[27] Kagan M Yu and Kugel K I 2001 *Usp. Fiz. Nauk.* **171** 577
Kagan M Yu and Kugel K I 2001 *Phys.—Usp.* **44** 553 (Engl. Transl.)
[28] Kugel K I, Rakhmanov A L and Sboychakov A O 2005 *Phys. Rev. Lett.* **95** 267210
Sboychakov A O, Kugel K I and Rakhmanov A L 2006 *Phys. Rev.* B **74** 014401
[29] Sboychakov A O, Kugel K I and Rakhmanov A L 2007 *Phys. Rev.* B **76** 195113
[30] Fratini M, Poccia N and Bianconi A 2008 *J. Phys.: Conf. Ser.* **108** 012036
[31] Bianconi A, Bianconi G, Caprara S, Di Castro D, Oyanagi H and Saini N L 2000 *J. Phys.: Condens. Matter* **12** 10655
[32] Di Castro D, Bianconi G, Colapietro M, Pifferi A, Saini N L, Agrestini S and Bianconi A 2000 *Eur. Phys. J.* B **18** 617
[33] Bianconi A, Agrestini S, Bianconi G, Di Castro D and Saini N L 2001 *J. Alloys Compounds* **317/318** 537
[34] Aeppli G, Mason T E, Hayden S M, Mook H A and Kulda J 1997 *Science* **278** 1432
[35] Dagotto E 2005 *Science* **309** 257
[36] Gorkov L P and Teitelbaum G B 2006 *Phys. Rev. Lett.* **97** 247003
[37] Löw U, Emery V J, Fabricius K and Kivelson S A 1994 *Phys. Rev. Lett.* **72** 1918
[38] Ortix C, Lorenzana J and Di Castro C 2008 arXiv:0801.0955
[39] Lorenzana J, Castellani C and Di Castro C 2001 *Phys. Rev.* B **64** 235127
[40] Lorenzana J, Castellani C and Di Castro C 2002 *Europhys. Lett.* **57** 704
[41] Sboychakov A O, Savel'ev S, Rakhmanov A L, Kugel K I and Nori F 2008 *Phys. Rev.* B **77** 224504